Understanding the Impact of Land Subsidence on Flooding in the Southeast Texas Coastal Region using PS-InSAR

Arip Syaripudin Nur, S.M.ASCE[1] and Yong Je Kim[2]*

[1]Graduate Student, Department of Civil and Environmental Engineering, Lamar University, Beaumont, TX 77710. E-mail: anur@lamar.edu
[2]Assistant Professor, Department of Civil and Environmental Engineering, Lamar University, Beaumont, TX 77710. E-mail: ykim3@lamar.edu (*corresponding author)

ABSTRACT

Due to its geographic location and geologic conditions, the southeast Texas (SETX) coast has been exposed to geological hazards, including land subsidence, floods, and coastal erosion. This study aimed to assess recent subsidence area and rate to understand their impact on flooding in SETX. The Persistent Scatterer Interferometric Synthetic Aperture Radar (PS-InSAR) method was applied in the study area using Sentinel-1 SAR satellite data during ascending observation from January 2020 to March 2023. The results showed that subsidence areas were observed over northwestern Houston of up to 2 cm/year. The results were consistent with GPS and groundwater level data. The study highlights the significant temporal and spatial variations subsidence rates, largely influenced by local groundwater extraction practices. By advocating the integration of InSAR, GPS, and groundwater measurements, this study aims to contribute to the mitigating subsidence and flood hazards in the SETX area.

INTRODUCTION

Land subsidence has emerged as a significant urban geological hazard, exacerbating the risk of floods, and posing a threat to critical infrastructure such as roads, bridges, sea walls, levees, and underground utility pipes (Kearns et al., 2015). Therefore, addressing the challenges posed by land subsidence has become imperative and costly. The southeast Texas (SETX) coast, due to its geographical location and geologic conditions, is particularly susceptible to geological hazards including land subsidence, floods, and coastal erosion (Miller and Shirzaei, 2019; Wang et al., 2017). The SETX coast intersects with three primary fault zones: the Hockley–Conroe Fault System, the Addicks Fault System, and the Long Point–Eureka Heigh (Khan et al., 2014). These fault systems traverse Holocene and Paleocene sediments and exhibit aseismic creep, resulting in temporal variations (Khan et al., 2022). Excessive groundwater extraction and sediment compaction are considered significant contributors to subsidence (Paine, 1993; Wang et al., 2020). Recognizing the magnitude of the problem, the Government of Texas and the United States Geological Survey (USGS) established the Harris-Galveston Subsidence District (HGSD) in 1975, followed by the formation of subsidence districts in the surrounding counties. To monitor and mitigate land subsidence, HGSD and USGS have implemented borehole extensometers and established an extensive groundwater monitoring network (Greuter, 2023). Additionally, in collaboration with the National Geodetic Survey (NGS), HGSD has developed a leveling survey and a Global Navigation Satellite System (GNSS) network.

Previous investigations have utilized interferometric synthetic aperture radar (InSAR) techniques to assess land subsidence in the SETX region, encompassing Houston and its surrounding areas. Qu et al., (2015) employed data from European Remote Sensing (ERS-1) and ERS-2 satellites to determine a subsidence rate of 53 mm/year for the period spanning 1993 to 2000. Furthermore, using observations from Envisat and the Advance Land Observation Satellite (ALOS), they identified subsidence rates of up to 30 mm/year from 2004 to 2011. Miller & Shirzaei (2019) conducted measurements utilizing ALOS data (2007-2011) and Sentinel-1A/B (2015-2017), revealing subsidence rates of up to 49 mm/year and 34 mm/year, respectively. Additionally, Khan et al. (2022) processed data from Sentinel-1 satellite from 2016 to 2020 and measured determining subsidence reaching up to 9 cm in magnitude.

The primary objective of this study is to delineate the extent of land subsidence in specific regions of SETX, particularly Harris County and Galveston County, along with their surrounding areas. Furthermore, the study aims to quantify the recent subsidence rates using time series analysis in order to understand the implications for flooding. To achieve this goal, this study employed the Persistence Scatterer Interferometric Synthetic Aperture Radar (PS-InSAR) method, utilizing Sentinel-1 SAR satellite data acquired during descending observations spanning from January 2020 to March 2022. Additionally, the study conducted a comparative analysis of subsidence rates obtained through InSAR measurements with data derived from global positioning system (GPS) measurements and aquifer water levels. By incorporating these diverse measurement techniques, the study highlights the significance of integrating InSAR, GPS, and groundwater observations in the development of flood resilience strategies.

MATERIALS AND METHODS

The analysis of land subsidence areas and rates in the SETX region utilized Sentinel-1 SAR C-band data, which operates at a wavelength of 5.54 cm and is managed by the European Space Agency (ESA). Figure 1 presents the SAR coverage of the study area, represented by a red rectangle, as well as the distribution of GPS stations (red dots) across SETX. Specifically, the study area falls within path 143 and frame 492. A total of 152 Sentinel-1 single look complex (SLC) images were collected for this study, employing the interferometric wide-swath (IW) mode and vertical transmission and vertical return (VV) polarization mode during the descending observation period spanning from January 2020 to March 2023 (Table 1). The datasets were sourced from the Alaska Satellite Facilities (ASF) and each scene underwent preprocessing using the Sentinel Application Platform (SNAP) tool.

Table 1. Acquisition dates of Sentinel-1 datasets during descending observation.

No	Date (yyyymmdd)	No	Date	No	Date	No	Date	No	Date	No	Date
1	20200105	27	20200615	53	20201124	79	20210511	105	20211020	131	20220705
2	20200111	28	20200621	54	20201130	80	20210517	106	20211026	132	20220717
3	20200117	29	20200627	55	20201206	81	20210523	107	20211101	133	20220729
4	20200123	30	20200703	56	20201212	82	20210529	108	20211107	134	20220810
5	20200204	31	20200709	57	20201218	83	20210604	109	20211113	135	20220822
6	20200210	32	20200715	58	20201224	84	20210610	110	20211119	136	20220915
7	20200216	33	20200721	59	20201230	85	20210616	111	20211125	137	20220927

8	20200222	34	20200727	60	20210111	86	20210622	112	20211201	138	20221009
9	20200228	35	20200802	61	20210117	87	20210628	113	20211207	139	20221021
10	20200305	36	20200808	62	20210123	88	20210704	114	20211213	140	20221102
11	20200311	37	20200814	63	20210129	89	20210710	115	20211219	141	20221114
12	20200317	38	20200826	64	20210204	90	20210716	116	20211225	142	20221126
13	20200323	39	20200901	65	20210210	91	20210722	117	20220106	143	20221208
14	20200329	40	20200907	66	20210216	92	20210803	118	20220130	144	20221220
15	20200404	41	20200913	67	20210222	93	20210809	119	20220211	145	20230101
16	20200410	42	20200919	68	20210228	94	20210815	120	20220223	146	20230113
17	20200416	43	20200925	69	20210306	95	20210821	121	20220307	147	20230125
18	20200422	44	20201001	70	20210312	96	20210827	122	20220319	148	20230206
19	20200428	45	20201007	71	20210318	97	20210902	123	20220331	149	20230218
20	20200504	46	20201013	72	20210324	98	20210908	124	20220412	150	20230302
21	20200510	47	20201019	73	20210330	99	20210914	125	20220424	151	20230314
22	20200516	48	20201025	74	20210405	100	20210920	126	20220506	152	20230326
23	20200522	49	20201031	75	20210411	101	20210926	127	20220518		
24	20200528	50	20201106	76	20210417	102	20211002	128	20220530		
25	20200603	51	20201112	77	20210429	103	20211008	129	20220611		
26	20200609	52	20201118	78	20210505	104	20211014	130	20220623		

A SAR image was selected as a reference image to coregister another SAR image. This coregistration process was carried out with at subpixel accuracy, creating interferometric pairs and resampling the images to ensure perfect matching. Subsequently, the coregistered images were cropped, resulting in images that only contain the specific region of interest. These images were then utilized to generate interferograms, capturing phase changes (interferences) and producing Interferometric SAR (InSAR) images. To obtain Differential Interferograms (DInSAR) images that exclusively depict deformation phases, these interferograms were subtracted with the topographic phase, which was derived from a 30-meter spatial resolution Digital Elevation Model (DEM) obtained from Copernicus DEM.

A reference image was selected on April 23, 2021, and used to generate a total of 153 interferograms. These interferograms, representing Differential Interferograms (DInSAR), were subsequently loaded into the StaMPS module for further processing. Initially, an iterative procedure was employed to estimate the phase noise value for each potential pixel in every interferogram. Pixels were then selected based on their noise characteristics, allowing for the estimation of the percentage of random (non-PS) pixels within the scene and enabling the calculation of density per km^2 (Hung et al., 2011). Following that, a threshold value of 0.4 was applied to weed out pixels that contributed to signals from neighboring ground resolution elements or were excessively noisy (Hooper et al., 2012). The threshold value also was considered to primarily eliminate areas over water and heavily decorrelated pixels in vegetated areas (Sousa et al., 2011). The wrapped phase of the selected pixels was corrected for spatially uncorrelated look angle error using a Digital Elevation Model (DEM). Subsequently, a 3D unwrapping method was employed to unwrap the phase, ensuring accuracy and continuity. See Hooper et al. (2007) for details. Unwrapped phases were examined, and any instances of unwrapping errors were identified

and discarded. The final step involved calculating the spatially correlated look angle (SCLA) error, primarily caused by spatially correlated DEM errors. Additionally, phase errors caused by atmospheric and orbit factors were simultaneously estimated. By subtracting the SCLA error image from the unwrapped phase, a mean deformation image was obtained. Furthermore, time-series analysis was performed, generating line-of-sight (LOS) measurements to capture temporal changes in surface deformation.

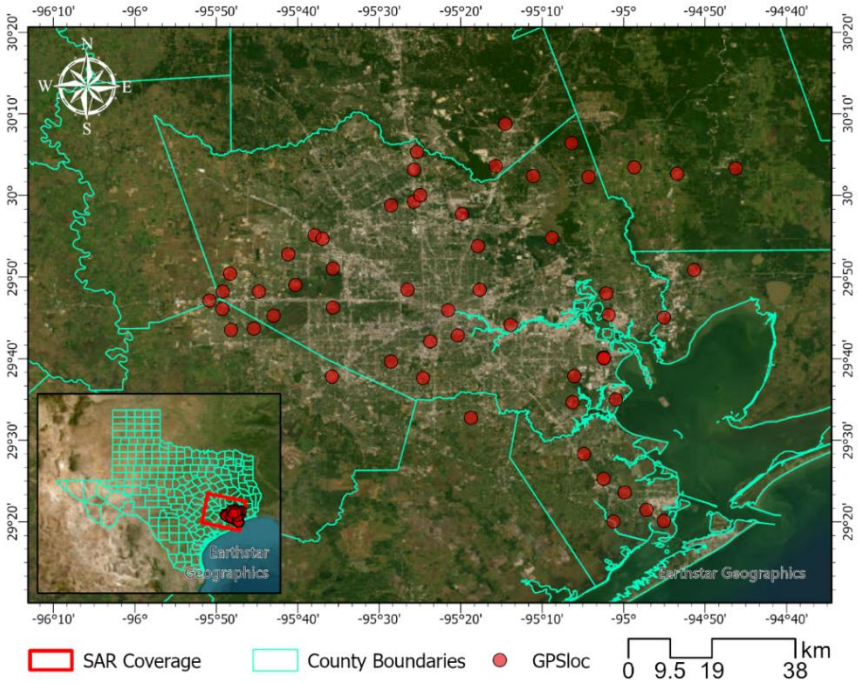

Figure 1. Map of study area showing the SAR coverage area and locations of GPS stations.

According to (Kearns et al., 2019), it is suggested that there is approximately horizontal movement of ~2mm/year with no consistent pattern observed in most of the Houston area. Consequently, assuming minimal horizontal deformation that can be disregarded, the majority of the line-of-sight (LOS) velocity can be attributed to vertical deformation. The relationship between LOS deformation and subsidence (vertical deformation) can be described by Equation 1.

$$S = -\frac{d}{cos\theta_i} \tag{1}$$

Where S represents the subsidence, d denotes the line-of-sight deformation, and θ_i indicates the incident angle (34 degrees) (Nur et al., 2020; Yastika et al., 2019). It's worth noting that the negative sign indicates land subsidence at that particular point.

The Gulf Coast Program of the U.S. Geological Survey Texas Water Science Center is responsible for collecting, processing, and interpreting groundwater level and GPS data. The primary objective of this program is to gain a comprehensive understanding of the impact of groundwater extraction on land subsidence in the Houston Galveston region of Texas. By analyzing these data sets, the program aims to assess and monitor changes in groundwater levels and their correlation with land subsidence phenomena in the area.

RESULTS AND DISCUSSION

The application of the time-series InSAR technique using the StaMPS algorithm resulted in the generation of 4,320,006 measurement points (MP). Figure 2 displays the mean deformation map depicting the subsidence patterns across the SETX area, derived from InSAR data spanning from January 2020 to March 2023. The color gradient from blue to red represents an increasing subsidence rate of up to 2 cm/year. Consistent with the expected outcomes of the PSInSAR method, specifically the StaMPS algorithm utilized in this study, a higher concentration of measurement points was observed in urban areas, while there were fewer points in vegetated or agricultural regions. Subsidence areas were observed over northwestern Houston and Katy experiencing high subsidence rates of up to 2 cm/year. Notable small areas with substantial subsidence rate were also identified in Bayton, eastern Houston.

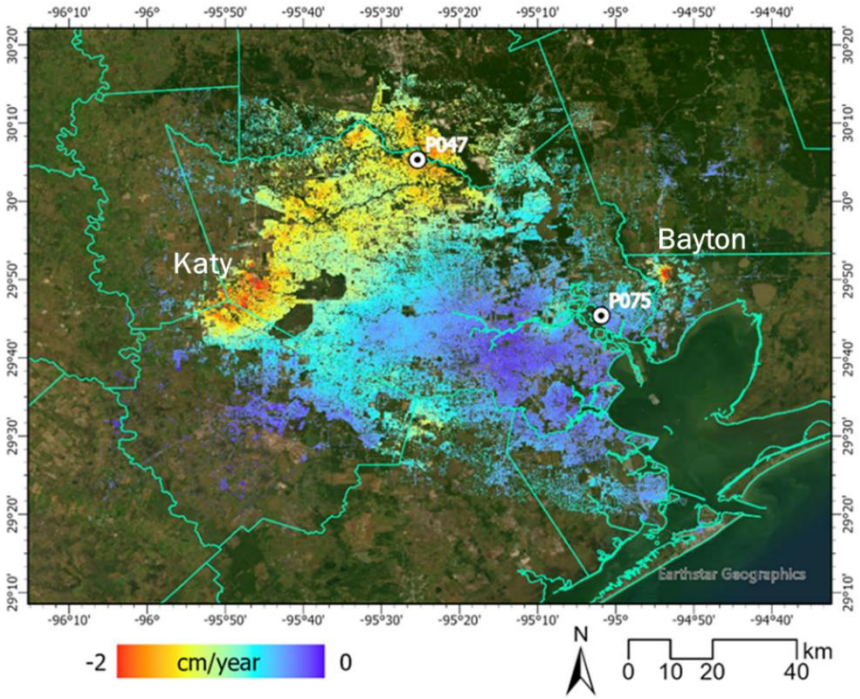

Figure 2. Mean vertical deformation map over SETX area using Sentinel-1 data from January 2020 to March 2023.

To generate the time series surface deformation, the average of the measurement points (MPs) within a 100-meter radius from a specific location was computed. These results were then compared with the GPS measurements obtained from station P047 and station P075, as depicted in Figure 3a and 3b, respectively. At station P047, the subsidence rate from 2020 to 2021 was determined to be 1.02 cm/year based on the GPS measurements. In comparison, the SAR measurement indicated a subsidence rate of 0.96 cm/year during the same period. The SAR measurements revealed that the subsidence continued in 2021, with a rate increasing up to 1.12 cm/year. On the other hand, the time series surface deformation at station P075 remained relatively stable, as observed from both the GPS station and SAR measurements.

The Gulf Coast Aquifer System covers the entire Texas coastline and is a complex, multilevel groundwater system (Khan et al., 2022). It consists of over 3600 meters of clay, silt,

sand, and gravel deposits, comprising several aquifers and confining systems. The aquifer system includes the Evangeline aquifer system, Catahoula confining system, Jasper aquifer, Burkville confining system, and Chicot aquifer. The Chicot and Evangeline aquifers are the primary sources of water for cities near the coast. Ground subsidence in the region was first observed in the early 1900s. Over-pumping of the Evangeline and Chicot aquifers has led to declines in water levels in certain sections of Houston, with a significant impact by 1977. By 1979, the land had subsided by approximately three meters. Figure 4 illustrates the changes in water-level altitudes above sea level in the Chicot and Evangeline aquifers from 1990 to 2021 (Ramage, 2022).

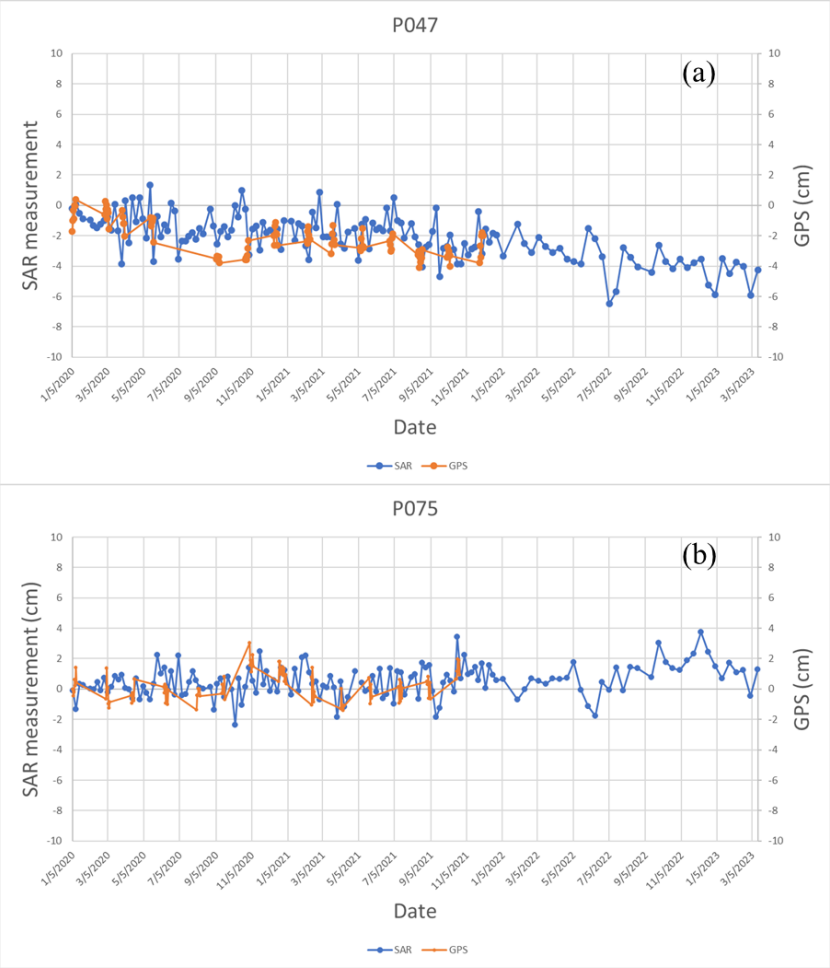

Figure 3. Comparison between time-series GPS station (a) P047 and (b) P075 with StaMPS measurement.

The water level changes in the Chicot and Evangeline aquifers exhibit varying contours, ranging from an 80-meter decline to a 40-meter rise. Four distinct areas of rapid groundwater decline, known as decline bowls, can be observed in both aquifers. These decline bowls are located in Katy, Rose Hill, Egypt, and Woodland. Additionally, a broader area of water-level rise is evident in central Houston, Friendswood, and La Porte. Interestingly, areas with high subsidence rates closely correspond to regions with declining groundwater levels, particularly in the Katy and Woodland areas. This pattern suggests a correlation between changes in groundwater levels and the occurrence of subsidence.

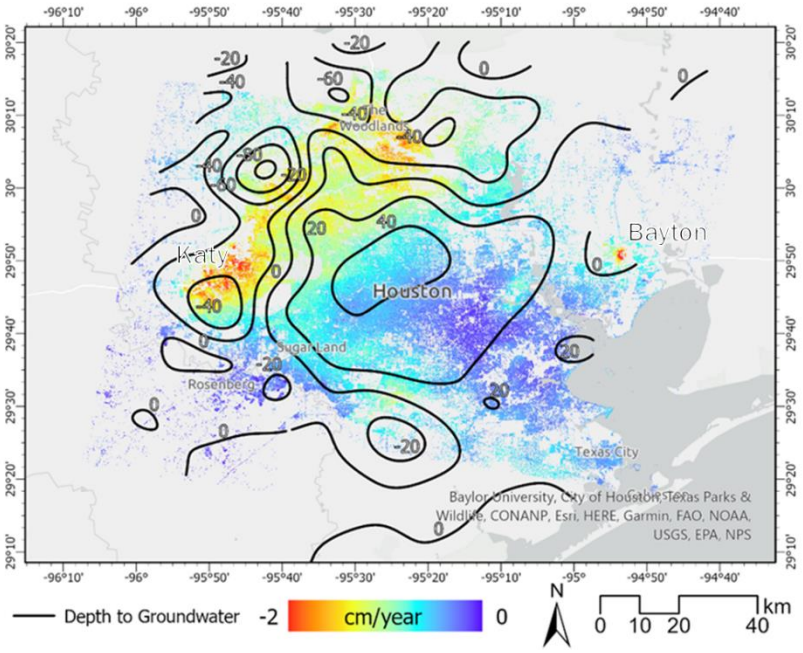

Figure 4. Contours showing the changes of groundwater levels in Chicot and Evangeline aquifers at the end of 2021.

In Figure 5, the time-series analysis of groundwater level changes at station P047 and station P075 provides valuable insights into the relationship between water-level fluctuations and subsidence areas. Figure 5a specifically demonstrates a declining trend in water level at station P047 starting from April 2021. During this period, the water level depleted from 50.67 meters below the surface to 61.52 meters. In contrast, at station P075 (Figure 5b), the water level remained relatively stable, ranging between 23 meters to 24 meters. These observations align with the time-series vertical deformation obtained from the PS-InSAR measurements. The correlation between water-level changes and temporal subsidence patterns can be inferred from these findings. The declining water level at station P047 corresponds to subsidence activity, as indicated by the PS-InSAR measurements. Conversely, the relatively stable water level at station P075 corresponds to minimal subsidence observed in that area. These results highlight the significance of monitoring groundwater levels as they provide valuable information regarding subsidence phenomena and their temporal patterns.

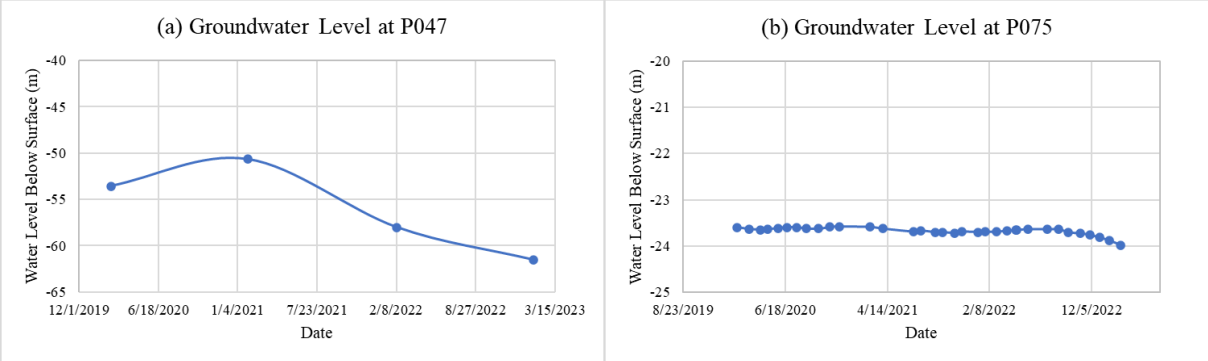

Figure 5. Time-series of groundwater level change at (a) station P047 and (b) station P075 from 2020 to 2023.

Figure 6 presents the National Flood Hazard Areas with mean vertical deformation map over the SETX area. The maps encompass a wide range of data, including hydrological factors such as flow rate, topographic slope, and elevation, as well as information on infrastructure, hydraulics, and land use (Federal Emergency Management Agency, 2022). The flood hazard map delineates areas with 1% annual chance flood hazard or 100 years floods, 0.2% annual chance flood hazard, also known as a 500-year flood, area with reduced risk due to levee systems, and regulatory floodway. It was observed that wide regions with high subsidence rates outside the designated flood hazard zones. A study conducted by (Miller and Shirzaei, 2019) found that 85% of the flooded area from Hurricane Harvey subsided at a rate of up to 5 mm/year. The study also revealed that the flooded areas appear to be affected by subsidence based on the Chi-square test analysis. Therefore, continued land subsidence within the study area has the potential to intensify flooding by compromising the flood control structures, altering floodplain boundaries and base flood drainage, and submerging wetlands. Additionally, the combination of land subsidence and rising sea level could further amplify flood hazard. By combining PS-InSAR techniques and GPS data a comprehensive understanding of vertical land motion can be obtained. Furthermore, the development of a more accurate hydrological model that incorporates subsidence observations can assist coastal cities in reevaluating flood risk zones and enhancing flood resilience.

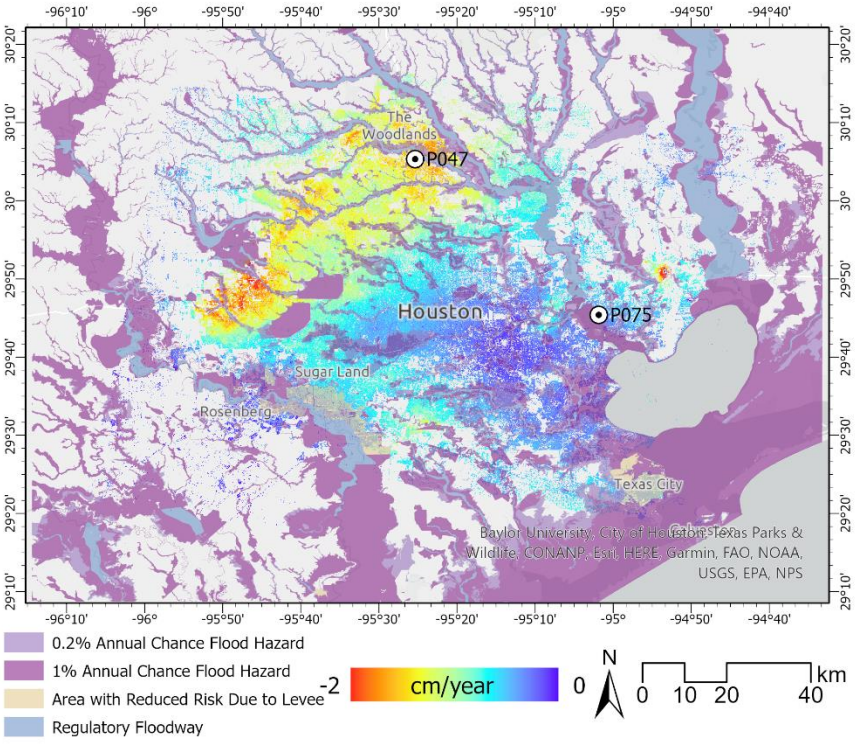

Figure 6. Flood risk zones provided by the National Flood Hazard Area (FEMA, 2022) displayed over mean vertical deformation map.

CONCLUSION

This study describes the significant land subsidence occurring in the SETX (Southeast Texas) region. The PS-InSAR measurements conducted from January 2020 to March 2023 revealed an alarming subsidence rate of up to 2 cm/year in the northwest and east areas. The

establishment of dense GPS and groundwater monitoring networks allowed for precise tracking of land subsidence and facilitated the assessment of the intricate relationship between groundwater withdrawals and subsidence. The results indicate that groundwater level changes are the primary contributing factor to land subsidence in the SETX region, as evidenced by their correlation with spatial and temporal subsidence patterns. Moreover, the study demonstrates that subsidence rates exhibit significant temporal and spatial variations, largely dependent on local groundwater withdrawal practices. Additionally, it is worth noting that flooding and storm events, exemplified by Hurricane Harvey, introduce the risk of flood-induced subsidence, further exacerbating the frequency and extent of flooding. These adverse consequences encompass damage to buildings, transportation infrastructure, and the environment. This study presents a comprehensive framework utilizing publicly available SAR data and GPS measurements, enabling precise monitoring of land subsidence with millimeter-level accuracy in urban areas. By advocating the application of InSAR, GPS, and groundwater measurements, this research strives to contribute to the reduction of subsidence and flood hazards in the SETX region.

REFERENCES

Federal Emergency Management Agency (FEMA). (2022). "National Flood Hazard Area". <https://hub.arcgis.com/datasets/esri::usa-flood-hazard-areas-2/about> (Jul. 1, 2023).

Greuter, A. (2023). *Determination of Groundwater Withdrawal and Subsidence in Harris and Galveston Counties*. Friendswood, Texas.

Hooper, A, Segall, P., Zebker, H. (2007). "Persistent scatterer interferometric synthetic aperture radar for crustal deformation analysis, with application to Volcán Alcedo, Galápagos". *Journal of Geophysical Research: Solid Earth*, 112(7), B07407. https://doi.org/10.1029/2006JB004763

Hooper, Andrew, Bekaert, D., Spaans, K., Arikan, M. (2012). "Recent advances in SAR interferometry time series analysis for measuring crustal deformation". *Tectonophysics*. https://doi.org/10.1016/j.tecto.2011.10.013

Hung, W. C., Hwang, C., Chen, Y. A., Chang, C. P., Yen, J. Y., Hooper, A., Yang, C. Y. (2011). "Surface deformation from persistent scatterers SAR interferometry and fusion with leveling data: A case study over the Choushui River Alluvial Fan, Taiwan". *Remote Sensing of Environment*, 115(4), 957–967. https://doi.org/10.1016/j.rse.2010.11.007

Kearns, T. J., Wang, G., Asce, M., Yan Bao, Jiang, J., Lee, D. (2015). "Current Land Subsidence and Groundwater Level Changes in the Houston Metropolitan Area (2005–2012)". *Journal of Surveying Engineering*, 141(4), 05015002. https://doi.org/10.1061/(ASCE)SU.1943-5428.0000147

Kearns, T. J., Wang, G., Turco, M., Welch, J., Tsibanos, V., Liu, H. (2019). "Houston16: A stable geodetic reference frame for subsidence and faulting study in the Houston metropolitan area, Texas, U.S". *Geodesy and Geodynamics*, 10(5), 382–393. https://doi.org/10.1016/J.GEOG.2018.05.005

Khan, S. D., Gadea, O. C. A., Tello Alvarado, A., Tirmizi, O. A. (2022). "Surface Deformation Analysis of the Houston Area Using Time Series Interferometry and Emerging Hot Spot Analysis". *Remote Sensing.*, 14(15), 3831. https://doi.org/10.3390/RS14153831

Khan, S. D., Huang, Z., Karacay, A. (2014). "Study of ground subsidence in northwest Harris county using GPS, LiDAR, and InSAR techniques". *Natural Hazards*, 73(3), 1143–1173. https://doi.org/10.1007/S11069-014-1067-X/FIGURES/13

Miller, M. M., Shirzaei, M. (2019). “Land subsidence in Houston correlated with flooding from Hurricane Harvey”. *Remote Sensing of Environment*, 225, 368–378. https://doi.org/10.1016/J.RSE.2019.03.022

Nur, A. S., Achmad, A. R., Lee, C. W. (2020). “Land Subsidence Measurement in Reclaimed Coastal Land: Noksan Using C-Band Sentinel-1 Radar Interferometry”. *Journal of Coastal Research*, 102(sp1), 218–223. https://doi.org/10.2112/SI102-027.1

Paine, J. G. (1993). “Subsidence of the Texas coast: inferences from historical and late Pleistocene sea levels”. *Tectonophysics*, 222(3–4), 445–458. https://doi.org/10.1016/0040-1951(93)90363-O

Qu, F., Lu, Z., Zhang, Q., Bawden, G. W., Kim, J. W., Zhao, C., Qu, W. (2015). “Mapping ground deformation over Houston–Galveston, Texas using multi-temporal InSAR”. *Remote Sensing of Environment*, 169, 290–306. https://doi.org/10.1016/J.RSE.2015.08.027

Ramage, J. K. (2022). *Depth to Groundwater Measured from Wells Completed in the Chicot and Evangeline (Undifferentiated) and Jasper Aquifers, Greater Houston Area, Texas, 2021*. Great Houston Area, Texas, 2021.

Sousa, J. J., Hooper, A. J., Hanssen, R. F., Bastos, L. C., Ruiz, A. M. (2011). “Persistent Scatterer InSAR: A comparison of methodologies based on a model of temporal deformation vs. spatial correlation selection criteria”. *Remote Sensing of Environment*, 115(10), 2652–2663. https://doi.org/10.1016/j.rse.2011.05.021

Wang, G., Asce, M., Turco, Michael, Soler, T., Kearns, T. J., Welch, J. (2017). “Comparisons of OPUS and PPP Solutions for Subsidence Monitoring in the Greater Houston Area”. *Journal of Surveying Engineering*, 143(4), 05017005. https://doi.org/10.1061/(ASCE)SU.1943-5428.0000241

Wang, G., Zhou, X., Wang, K., Ke, X., Zhang, Y., Zhao, R., Bao, Y. (2020). “GOM20: A Stable Geodetic Reference Frame for Subsidence, Faulting, and Sea-Level Rise Studies along the Coast of the Gulf of Mexico”. *Remote Sensing*, 12(3), 350. https://doi.org/10.3390/RS12030350

Yastika, P. E., Shimizu, N., Abidin, H. Z. (2019). “Monitoring of long-term land subsidence from 2003 to 2017 in coastal area of Semarang, Indonesia by SBAS DInSAR analyses using Envisat-ASAR, ALOS-PALSAR, and Sentinel-1A SAR data”. *Advances in Space Research*, 63(5), 1719–1736. https://doi.org/10.1016/j.asr.2018.11.008